Research Article

Saqib Murtaza, Poom Kumam*, Muhammad Bilal, Thana Sutthibutpong, Nopporn Rujisamphan, and Zubair Ahmad

Parametric simulation of hybrid nanofluid flow consisting of cobalt ferrite nanoparticles with second-order slip and variable viscosity over an extending surface

https://doi.org/10.1515/ntrev-2022-0533 received June 16, 2022; accepted March 9, 2023

Abstract: This study explores the unsteady hybrid nanofluid (NF) flow consisting of cobalt ferrite (CoFe₂O₄) and copper (Cu) nano particulates with natural convection flow due to an expanding surface implanted in a porous medium. The Cu and CoFe₂O₄ nanoparticles (NPs) are added to the base fluid water to synthesize the hybrid

* Corresponding author: Poom Kumam, Center of Excellence in Theoretical and Computational Science (TaCS-CoE), Faculty of Science, King Mongkut's University of Technology Thonburi (KMUTT), 126 Pracha Uthit Rd, Bang Mod, Thung Khru, Bangkok 10140, Thailand; Department of Medical Research, China Medical University Hospital, China Medical University, Taichung 40402, Taiwan, e-mail: poom.kum@kmutt.ac.th

Saqib Murtaza: Department of Mathematics, Faculty of Science, King Mongkut's University of Technology Thonburi (KMUTT), 126 Pracha Uthit Rd, Bang Mod, Thung Khru, Bangkok 10140, Thailand Muhammad Bilal: Department of Mathematics, Sheikh Taimur Academic Block-II, University of Peshawar, 25120, Khyber Pakhtunkhwa, Pakistan

Thana Sutthibutpong: Center of Excellence in Theoretical and Computational Science (TaCS-CoE), Faculty of Science, King Mongkut's University of Technology Thonburi (KMUTT), 126 Pracha Uthit Rd, Bang Mod, Thung Khru, Bangkok 10140, Thailand; Department of Physics, Theoretical and Computational Physics Group, King Mongkut's University of Technology Thonburi (KMUTT), 126 Pracha-Uthit Road, Bang Mod, Thung Khru, Bangkok 10140, Thailand

Nopporn Rujisamphan: Center of Excellence in Theoretical and Computational Science (TaCS-CoE), Faculty of Science, King Mongkut's University of Technology Thonburi (KMUTT), 126 Pracha Uthit Rd, Bang Mod, Thung Khru, Bangkok 10140, Thailand; Nanoscience and Nanotechnology Graduate Program, Faculty of Science, King Mongkut's University of Technology Thonburi (KMUTT), 126 Pracha-Uthit Road, Bang Mod, Thung Khru, Bangkok 10140, Thailand

Zubair Ahmad: Department of Mathematics and Physics, University of Campania Luigi Vanvitelli Caserta, 81100, Italy

NF. The effects of second-order velocity slip condition, chemical reaction, heat absorption/generation, temperature-dependent viscosity, and Darcy Forchheimer are also assessed in the present analysis. An ordinary differential equation system is substituted for the modeled equations of the problem. Further computational processing of the differential equations is performed using the parametric continuation method. A validation and accuracy comparison are performed with the Matlab package BVP4C. Physical constraints are used for presenting and reviewing the outcomes. With the increase in secondorder velocity slip condition and unsteady viscosity, the rates of heat and mass transition increase significantly with the variation in Cu and Fe₂O₄ NPs. The findings suggest that the uses of Cu and Fe₂O₄ in ordinary fluids might be useful in the aerodynamic extrusion of plastic sheets and extrusion of a polymer sheet from a dye.

Keywords: stretching surface, BVP4C, parametric continuation method, hybrid approach, slip conditions, chemical reaction.

Nomenclature

| $A=(\zeta/u_0)$ | unsteadiness coefficient |
|--|----------------------------|
| $\widetilde{\mathcal{C}}$ | concentration of the fluid |
| $\widetilde{\mathcal{C}}_{\infty}$ | concentration at infinity |
| $D_{ m hnf}$ | mass diffusion |
| $Fr = \frac{C_b}{k \star^{1/2}}$ | Forchheimer number |
| <i>g</i> | gravitational force |
| $\kappa = \frac{v_f(1-\zeta t)}{\kappa \tilde{u}_0}$ $k_{\rm hnf}$ | permeability constant |
| $k_{ m hnf}$ | thermal conductivity |
| Kr | chemical reaction |
| K_n | Knudsen number |
| N_0 | thermal slip term |
| $\Pr = \frac{v_f(\rho C_p)}{k_f},$ | Prandtl number |
| | |

2 — Saqib Murtaza et al. DE GRUYTER

| Q_0 | heat absorption/generation |
|---|--------------------------------------|
| R | varying viscosity |
| $Sc = \frac{v_f}{D_f}$ \widetilde{T} | Schmidt number |
| \widetilde{T} D_f | temperature of the fluid |
| $	ilde{T}_{	extsf{S}}$ | surface temperature |
| \widetilde{T}_{∞} | fluid temperature at infinity |
| \widetilde{u} | velocity component on <i>x</i> -axis |
| $\widetilde{u}_{	ext{slip}}$ | velocity slip |
| $ u_{ m hnf}$ | kinematic viscosity |
| $\widetilde{\mathcal{V}}$ | velocity component on y-axis |
| $\mu_{ m f}$ | dynamic viscosity of fluid |
| λ | free path molecular mean |
| α | momentum accommodation |
| | constant |
| $\mu_{ m hnf}$ | dynamic viscosity |
| $\beta = N_0 \sqrt{\tilde{u}_0/\nu_f}$ | thermal slip |
| $\gamma = a\sqrt{\tilde{u}_0/v_f}$ | slip velocity term of 1st-order |
| $\Gamma = ((1-\zeta t)Q_0/\tilde{u}_0(\rho C_p)_f)$ | heat source term |
| μ_0 | reference viscosity of carrier fluid |
| $ ho_{ m hnf}$ | density |
| $oldsymbol{eta}_{	ext{hnf}}$ | volumetric expansion |
| $(\rho C_p)_{\mathrm{hnf}}$ | specific heat capacity |
| $\delta = b(\tilde{u}_0/v_f)$ | slip velocity term of second-order |
| $\tau = (g\beta_t(\tilde{T}_b - \tilde{T}_s)/x\tilde{u}_0^2)$ | Grashof number |
| | |

1 Introduction

Various applications of fluid flow analysis across an extending sheet have been achieved in various sectors, including polymer manufacturing and aerodynamic extrusion of plastics and so on [1]. To simulate the behavior of simple and hybrid nanomaterials, Gul et al. [2] used a stretching sheet. Relative to simple nanofluids (NFs), the hybrid nanoliquid is more efficacious in heat conduction. Bilal *et al.* [3] documented the ferrofluid flow on a stretchy substratum with suction and injection influences. Puneeth et al. [4] evaluated the effects of mass transfer on the dynamics of a Casson hybrid NF on an asymmetrical nonlinear stretchy sheet. In a systematic review, Hussain et al. [5] investigated the heat transference properties of magneto-hydro-dynamic (MHD) nanofluid (NF) flow across an expanding surface. Rotation is known to promote heat flux, while lowering skin friction. Shuaib et al. [6] observed the fluid dynamics and heat distribution. As compared to a classical model, the fractional model seems to be more accurate. The poroelastic rotatory nanoliquid flow across a linearly increasing surface under magnetic impact was studied by Raza et al. [7]. The energy transmission through NF flow over a contracting sheet was considered by Uddin

et al. [8]. Rasool et al. [9] theoretically studied the Darcy-Forchheimer MHD NF flow with a non-linear extending sheet. The findings show that when the intensity of heat radiation increases, the thermal layer undergoes considerable changes in the progressive manner. An analysis of the effects of a 3D flow of Casson nano liquid over a Riga plate was published by Upreti et al. [10]. An analysis of Cu–Ag/H₂OC₂H₆O₂ hybrid NF flow was conducted by Joshi et al. [11]. They examined the considered phenomena in the presence of dissipation of viscosity. Upreti et al. [12] evaluated the nanoliquid flow between two parallel surfaces. They analyzed the entropy generation phenomena in the hybrid NF.

Hybrid NF is a revolutionary variant of liquid that surpasses regular fluids at energy transfers. Thermodynamic implications for hybrid NFs include chilling in elevated temperature [13]. In addition to renewable radiation, hybrid nuclear reactors are used in heating systems, heat exchangers, air conditioning units, automobiles, electrical refrigerators, turbines, radioactivity equipment, broadcasters, spacecraft, and biotech. Copper (Cu) and cobalt ferrite (CoFe₂O₄) NPs in the global solvent water are the purposes of this research. Electrodeposition, a "green" chemical approach, may be used to make Cu NPs from plant water extracts. New antitubercular medicines are being carried by Cu NPs [14]. Cu acts as an antiseptic, antibacterial, and antiviral ingredient when introduced to aquatic for varnishes, polymeric, and fibers. Cu-containing dietary supplements have a high absorption rate. Tensile strength is strong in Cu alloys and metals [15]. Metallic compounds encompass iron and cobalt NPs. Iron reduces interstitial endurance, permitting charge/ion mobility on the surface [16]. Imaging methods have shown to be critical in accurately identifying disorders. MRI is the most flexible of them all because it can give you morphological and physiological information. Bi-magnetic granules are used to make it more effective. Bi-magnetic NPs can be utilized for therapeutic agents and photoacoustic imaging, making them interesting candidates for development as enhanced MRI contrast agents. Bi-magnetic NPs can also be applied in therapeutic agents and photoacoustic imaging. Magnetic therapy is employed to cure tumors because cancerous cells are much more susceptible to less heat than normal tissues. Energy elevation produced by magnetic NPs accumulation can prevent cancer while exhibiting little consequences on adjacent tissues [17].

Numerous scientists and academics focus on the quantitative perspective to the abovementioned issues and challenges. Bilal *et al.* [18] evaluated the influence of electric and ferromagnetic effects on the hybrid NF flow across two rotary interfaces. The momentum boundary

layer is enhanced by the electric factor. A hybrid NF was assessed with CoFe₂O₄ and Fe₃O₄ in ethylene glycol by Ramesh *et al.* [19]. The results of metallic cushions and nanostructured materials were calculated with an MWCNT-Fe₃O₄ hybrid NF by Wang *et al.* [20]. Using a transparent extendable sheet with heat and momentum transitions, Bilal *et al.* [21] explored the effect of radiant energy on unsteady peristaltic flow. The distribution of microrotations is influenced by the porosity factor. In their study of NF flow, Algehyne *et al.* [22] used motile microbes and nanoparticles on porous moveable substrates. Few of the earlier studies [23–27] include some related literature of NFs and hybrid NFs.

The constant fluid physical parameters have been considered in various NF flow simulations. NFs, however, have variably viscous properties, which are critical to NF flow because they vary greatly with temperature. Internal resistance, for example, generates heat, which raises the temperature and hence influences the viscosity of NFs. To accurately assess the flow characteristics of NFs, it is crucial to take into account the viscosity-temperature discrepancy. Kuttan et al. [28] investigated the effects of temperature-dependent viscosity on fluid flow across a smooth surface. Shafiq et al. [29] investigated the NF flow on thin slandering needles. The authors dispersed carbon nanotubes in ethylene glycol to make homogenous suspension. Udawattha et al. [30] used the viscoelasticity of solid particle dispersion to determine the effective viscosity of NFs. There is currently a scarcity of data on the flow of Cu-CoFe₂O₄/H₂O hybrid NFs when temperature-dependent viscosity is considered.

There are many cases whereby a no-slip boundaries condition is not appropriate. For example, polymer melts exhibit some wall slips for distinct non-Newtonian fluids. and these slips tend to follow a monotonous and nonlinear relationship between slip velocity and adhesion friction mathematical problems [31]. Fluids with a slip boundary condition are beneficial in a range of technical and biomedical disciplines, including costly lubrication, optical coatings, cooling apparatus, purification of prosthetic heart valves, internal chambers, and other industrial operations. As a result, some researchers have looked into the implication of the slip boundary condition [32]. For instance, Oyelakin et al. [33] and Tlili et al. [34] investigated the impact of slip conditions on NF flow and energy conversion across a rigid sheet. Khan et al. [35] extensively documented the impact of slip conditions on NF flow. They discovered that when the value of second-order velocity slip conditions increases, the thermal allocation and thermal pressure gradient rise. However, nothing is known regarding the effect of second-order slip on the flow of Cu-C₀Fe₂O₄/H₂O

hybrid NFs overstretched surfaces. One of the goals of this research is to fill up the gaps in the previously mentioned information.

As a result of the abovementioned literature review, we examined the flow and heat transmission of Cu-C₀Fe₂O₄/ H₂O hybrid NF surfaces over stretching surfaces. In addition to temperature-dependent viscosity, heat source, free convection, Darcy Forchheimer, second-order slip, and chemical reaction are taken into account. A spectral parametric continuation method (PCM) is used to evaluate the governing equations. It is a highly accurate and fast-convergent method. Tables and graphs are also presented to illustrate how controlling factors affect hybrid NF flow velocity and temperature gradients. In biological domains, such as enzymatic biosensors, drug delivery, cancer therapy, and enzymatic biosensors, the proposed model has promising implications. So far, no assessment has been conducted on this topic. In comparison with other studies that have been conducted, this work is unique and innovative.

2 Mathematical formulation

We illustrated a 2D unsteady hybrid NF flow with velocity and thermal slip conditions passing over linearly extending texture embedded in the permeable medium. The Cu and CoFe_2O_4 nanoparticles are equally dispersed in water, to reform hybrid NF. The flow regime is y>0, where x-axis and y-axis are along the flow direction and normal to the flow field, respectively. Initially, the hybrid NF is at rest with a consistent temperature \tilde{T}_s at t=0. But at t>0, the surface starts stretching linearly with velocity $\tilde{u}_w=(\tilde{u}_0/1-\xi t)x$, where $\tilde{u}_0<0$ show surface shrinking and $\tilde{u}_0>0$ represent surface stretching. On behalf of the above presumption and Boussinesq approximation, the modeled equations for the fluid flow are calculated as follows [36,37]:

$$\frac{\partial \tilde{u}}{\partial x} + \frac{\partial \tilde{v}}{\partial y} = 0, \tag{1}$$

$$\begin{split} \rho_{\rm hnf} & \left(\frac{\partial \tilde{u}}{\partial t} + u \frac{\partial \tilde{u}}{\partial x} + v \frac{\partial \tilde{u}}{\partial y} \right) = \mu_{\rm hnf} \frac{\partial^2 \tilde{u}}{\partial y^2} + \frac{\partial \tilde{u}}{\partial y} \frac{\partial}{\partial y} (\mu_{\rm hnf}) \\ & - \frac{\mu_{\rm hnf}}{K} \tilde{u} + g \begin{pmatrix} (\rho \beta_t)_{\rm hnf} (\tilde{T} - \tilde{T}_s) + \\ (\rho \beta_c)_{\rm hnf} (\tilde{C} - \tilde{C}_s) \end{pmatrix} - F u^2, \end{split} \tag{2}$$

$$(\rho C_p)_{\text{hnf}} \left(\frac{\partial \tilde{T}}{\partial t} + \tilde{u} \frac{\partial \tilde{T}}{\partial x} + \tilde{v} \frac{\partial \tilde{T}}{\partial y} \right)$$

$$= k_{\text{hnf}} \frac{\partial^2 \tilde{T}}{\partial y^2} + Q_0 (\tilde{T} - \tilde{T}_{\infty}),$$
(3)

$$\left(\frac{\partial \tilde{C}}{\partial t} + \tilde{u}\frac{\partial \tilde{C}}{\partial x} + \tilde{v}\frac{\partial \tilde{C}}{\partial y}\right) = D_{\text{hnf}}\frac{\partial^2 C}{\partial y^2} + \text{Kr}(\tilde{C} - \tilde{C}_{\infty}).$$
(4)

The boundary conditions are as follows:

$$\tilde{u}(x, t) = \tilde{u}_w + \tilde{u}_{\text{slip}}, \ \tilde{v} = 0, \ \tilde{T} = \tilde{T}_b + N_0 \frac{\partial \tilde{T}}{\partial y},
C = C_b \text{ at } y = 0,
\tilde{u}(x, t) \to 0, \ \tilde{v} \to 0, \ \tilde{T} \to \tilde{T}_s, \ C \to C_s \text{ as } y \to \infty$$

$$\tilde{u}(x, t) = \tilde{u}_w + \tilde{u}_{\text{slip}}, \ \tilde{v} = 0, \ \tilde{u} = \frac{\tilde{u}_0}{1 - \zeta t} x f'(\zeta), \ \tilde{v} = \sqrt{\frac{\tilde{u}_0 v_f}{1 - \zeta t}} f(\zeta),$$

$$\tilde{u}(x, t) \to 0, \ \tilde{v} \to 0, \ \tilde{T} \to \tilde{T}_s, \ C \to C_s \text{ as } y \to \infty$$

$$\tilde{u}(x, t) \to 0, \ \tilde{v} \to 0, \ \tilde{T} \to \tilde{T}_s, \ C \to C_s \text{ as } y \to \infty$$
The similarity variables are as formula (variables).

where $ho_{
m hnf}$, $ho_{
m hnf}$, $ho_{
m hnf}$, and $ho_{
m hnf}$ show density, dynamic viscosity, mass diffusivity, and kinematic viscosity of hybrid NF. Here N_0 , Q_0 , $\beta_{\rm hnf}$, Kr, and g are the thermal slip term, heat absorption/generation, volumetric expansion of hybrid NF, chemical reaction, and gravitational force, respectively.

$$\mu_{\rm f} = \mu_0 e^{-R\theta(\zeta)},\tag{6}$$

$$\tilde{u}_{\rm slip} = a \frac{\partial \tilde{u}}{\partial v} + b \frac{\partial^2 \tilde{u}}{\partial v^2},\tag{7}$$

where a and b are expressed as follows:

$$a = \frac{2}{3} \left(\frac{3 - \alpha r^2}{\alpha} - \frac{3}{2} \frac{1 - r^2}{K_n} \right) \lambda,$$

$$ab = -\frac{1}{4} \left(r^4 + \frac{2}{K_n^2} (1 - r^2) \right) \lambda^2 \right\}.$$
(8)

Table 1: Experimental values of Cu, CoFe₂O₄, and water [38]

| | $ ho({ m kg/m^3})$ | $C_p(J/kg K)$ | <i>k</i> (W/mK) |
|-------------|--------------------|---------------|-----------------|
| Water | 997.1 | 4,179 | 0.613 |
| Cu | 8,933 | 385 | 401 |
| $CoFe_2O_4$ | 4,907 | 700 | 3.7 |

Here λ is the free path molecular mean and K_n is the Knudsen number. R is the varying viscosity (R < 0 for liquid & R > 0 for gas), and μ_0 is the reference viscosity of carrier fluid (Tables 1 and 2).

The similarity variables are as follows:

$$\tilde{u} = \frac{\tilde{u}_0}{1 - \zeta t} x f'(\zeta), \quad \tilde{v} = \sqrt{\frac{\tilde{u}_0 v_f}{1 - \zeta t}} f(\zeta),$$

$$\zeta = \sqrt{\frac{\tilde{u}_0}{v_f (1 - \zeta t)}} y, \quad \varphi(\zeta) = \frac{\tilde{C} - \tilde{C}_s}{\tilde{C}_b - \tilde{C}_s}, \quad \theta(\zeta) = \frac{\tilde{T} - \tilde{T}_s}{\tilde{T}_b - \tilde{T}_s} \right\}. \tag{9}$$

Substituting equation (8) in equations (1)–(7), we get

$$f'''(\zeta) + \wp_1 \wp_2 \left(f(\zeta) f''(\zeta) - A \left(f'(\zeta) + \frac{\zeta}{2} f''(\zeta) \right) - f'^2(\zeta) + \wp_3 \tau \theta(\zeta) \right)$$

$$- R\theta'(\zeta) - \kappa f'(\zeta) \operatorname{Fr} = 0.$$
(10)

$$\frac{k_{\text{hnf}}}{k_{\text{f}}}\theta''(\zeta) + \wp_{4} \text{Pr} \left(f(\zeta)\theta'(\zeta) - A \left(2\theta(\zeta) + \frac{\zeta}{2}\theta'(\zeta) \right) \right) (11)$$

$$+ \text{Pr } \Gamma \theta(\zeta) = 0,$$

$$\frac{D_{\text{hnf}}}{D_{6}} \frac{1}{\text{Sc}} \varphi'' + Af\varphi' - Kc\varphi = 0.$$
(12)

The transform conditions are as follows:

$$f(0) = 0, f'(0) = 1 + \delta f'''(0) + \gamma f''(0),$$

$$\theta(0) = 1 + \beta \theta'(0), \varphi(0) = 1,$$

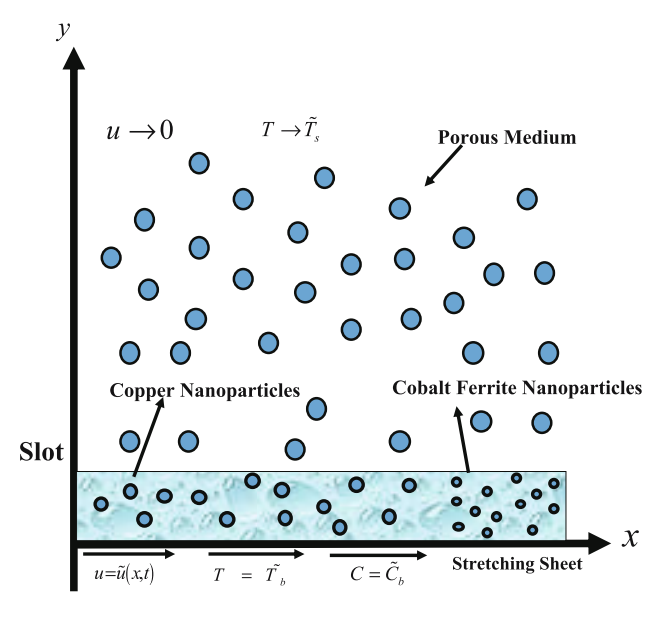
$$f'(\infty) \to 0, \theta(\infty) \to 0, \varphi(\infty) \to 0$$
(13)

Here

$$\wp_1 = \frac{\mu_{\text{hnf}}}{\mu_{\text{hf}}}, \, \wp_2 = \frac{\rho_{\text{hnf}}}{\rho_{\text{hf}}}, \, \wp_3 = \frac{k_{\text{hnf}}}{k_{\text{bf}}}, \, \wp_4 = \frac{(\rho C_p)_{\text{hnf}}}{(\rho C_p)_{\text{bf}}}, \quad (14)$$

Table 2: Mathematical model for hybrid nanoliquid ($\phi_1 = \phi_{Cu}$, $\phi_2 = \phi_{CoFe_2O_4}$) [38]

Properties $\frac{\mu_{\text{hnf}}}{\mu_{\text{hf}}} = \frac{1}{(1 - \phi_{\text{Cu}} - \phi_{\text{CoFe}_2O_4})^2}$ Viscosity Density $\frac{\rho_{\text{hnf}}}{\rho_{\text{bf}}} = \phi_{\text{Cu}} \left(\frac{\rho_{\text{Cu}}}{\rho_{\text{bf}}} \right) + \phi_{\text{CoFe}_2\text{O}_4} \left(\frac{\rho_{\text{CoFe}_2\text{O}_4}}{\rho_{\text{bf}}} \right) + (1 - \phi_{\text{Cu}} - \phi_{\text{CoFe}_2\text{O}_4})$ $\frac{(\rho C_p)_{hnf}}{(\rho C_p)_{hf}} = \phi_{Cu} \left(\frac{(\rho C_p)_{Cu}}{(\rho C_p)_{bf}} \right) + \phi_{CoFe_2O_4} \left(\frac{(\rho C_p)_{CoFe_2O_4}}{(\rho C_p)_{hf}} \right) + (1 - \phi_{Cu} - \phi_{CoFe_2O_4})$ Thermal capacity Thermal conductivity $\frac{\left(\frac{\phi_{\text{Cu}}k_{\text{Cu}} + \phi_{\text{CoFe}2O_4}k_{\text{CoFe}2O_4}}{\phi_{\text{Cu}} + \phi_{\text{CoFe}2O_4}}\right) + 2k_{\text{bf}} + 2(\phi_{\text{Cu}}k_{\text{Cu}} + \phi_{\text{CoFe}2O_4}k_{\text{CoFe}2O_4}) - 2(\phi_{\text{Cu}} + \phi_{\text{COFe}2O_4})k_{\text{bf}}}{\phi_{\text{Cu}} + \phi_{\text{CoFe}2O_4}k_{\text{CoFe}2O_4}}\right) + 2k_{\text{bf}} - 2(k_{\text{Cu}}\phi_{\text{Cu}} + k_{\text{COFe}2O_4}\phi_{\text{CoFe}2O_4}) + (\phi_{\text{Cu}} + \phi_{\text{CoFe}2O_4})2k_{\text{bf}}}$ **Electrical conductivity** $\underbrace{\frac{\phi_{\text{Cu}}\sigma_{\text{Cu}} + \sigma_{\text{CoFe}_2\text{O}_4}\phi_{\text{CoFe}_2\text{O}_4}}{\phi_{\text{CoFe}_2\text{O}_4} + \phi_{\text{Cu}}}}_{\text{Cu}} + 2\sigma_{\text{bf}} + 2(\phi_{\text{Cu}}\sigma_{\text{Cu}} + \phi_{\text{CoFe}_2\text{O}_4}\sigma_{\text{CoFe}_2\text{O}_4}) - 2(\phi_{\text{Cu}} + \phi_{\text{CoFe}_2\text{O}_4})\sigma_{\text{bf}}}_{\text{Cu}}$ $\frac{\phi_{\text{Cu}}\sigma_{\text{Cu}} + \phi_{\text{CoFe}_2\text{O}_4}\sigma_{\text{CoFe}_2\text{O}_4}}{A_{-} + A_{-} - A_{-}} + 2\sigma_{\text{bf}} - (\phi_{\text{Cu}}\sigma_{\text{Cu}} + \phi_{\text{CoFe}_2\text{O}_4}\sigma_{\text{CoFe}_2\text{O}_4}) + (\phi_{\text{Cu}} + \phi_{\text{CoFe}_2\text{O}_4})\sigma_{\text{bf}}$



 $Cu + CoFe \ o + water = Hybrid \ Nanofluid$

Figure 1: Physical sketch of the hybrid NF flow through stretching sheet.

where $\Pr = \frac{v_f(\rho C_p)}{k_f}$, is the Prandtl number, $\Pr = \frac{C_b}{k^{\star 1/2}}$ is the Darcy Forchheimer number, $Sc = \frac{v_f}{D_f}$ is the Schmidt number, $\beta = N_0 \sqrt{\tilde{u}_0/v_f}$ is the thermal slip, $\delta = b(\tilde{u}_0/v_f)$ is the slip velocity term of second-order, $\gamma = a\sqrt{\tilde{u}_0/v_f}$ is the slip velocity term of first-order, $\tau = (g\beta_t(\tilde{T}_b - \tilde{T}_s)/b\tilde{u}_0^2)$ is the Grashof number, $\Gamma = ((1 - \zeta t)Q_0/\tilde{u}_0(\rho C_p)_f)$ is the heat source, $A = (\zeta/u_0)$ is the unsteadiness coefficient, and $\kappa = \frac{v_f(1-\zeta t)}{K\tilde{u}_0}$ is the permeability constant.

The non-dimensional physical interest quantities are as follows:

$$Re_{x}^{1/2}C_{fx} = \frac{f''(0)}{(1 - \phi_{1})^{2.5}(1 - \phi_{2})^{2.5}},$$

$$Re_{x}^{1/2}Nu_{x} = \frac{k_{\text{hnf}}}{k_{\text{f}}}\theta'(0), Re_{x}^{1/2}Sh_{x} = -\varphi'(0).$$
(15)

3 Numerical solution

The basic steps while using PCM are as follows [39,40].

Step 1: Simplifying the BVP to a 1st system of ordinary differential equations (ODEs)

$$h_1 = f(\zeta), \ h_2 = f'(\zeta), \ h_3 = f''(\zeta), \ h_4 = \theta(\zeta),$$

$$h_5 = \theta'(\zeta), \ h_6 = \varphi(\zeta), \ h_7 = \varphi'(\zeta).$$
(16)

By substituting equation (9) in equations (1)–(5), we get

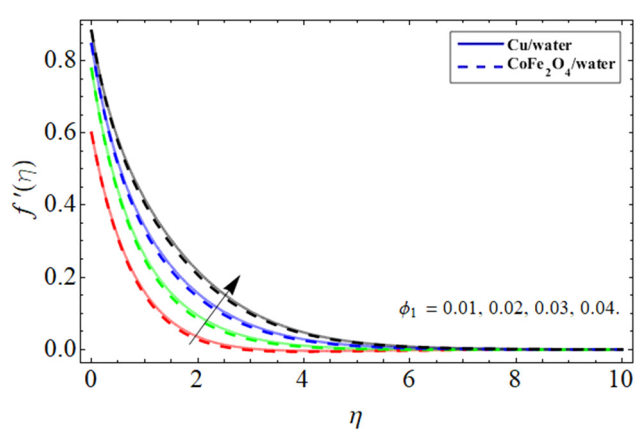


Figure 2: Velocity outlines $f'(\eta)$ vs Cu NPs.

$$\hbar'_{3} + \wp_{1}\wp_{2}\left(\hbar_{1}\hbar_{3} - A\left(\hbar_{2} + \frac{\zeta}{2}\hbar_{3}\right) - \hbar_{2}^{2} + \wp_{3}\tau \,\,\hbar_{4}\right) - R\hbar_{5}$$

$$- \kappa \hbar_{2}Fr = 0,$$
(17)

$$\frac{k_{\text{hnf}}}{k_f}\hbar'_5 + \wp_4 \Pr\left(\hbar_1 \hbar_5 - A\left(2\hbar_4 + \frac{\zeta}{2}\hbar_5\right)\right) + \Pr\Gamma \hbar_4 = 0, \quad (18)$$

$$\frac{D_{\rm hnf}}{D_{\rm f}} \frac{1}{{\rm Sc}} h'_7 + Af h_7 - Kc h_6 = 0. \tag{19}$$

The transform conditions are as follows:

$$h_1(0) = 0, \ h_2(0) = 1 + \gamma h_3(0) + \delta h'_3(0),
h_4(0) = 1 + \beta h_5, \ h_6(0) = 1,
h_2(\infty) \to 0, \ h_4(\infty) \to 0, \ h_6(\infty) \to 0.$$
(20)

Step 2: Introducing parameter p

$$h'_{3} + \wp_{1}\wp_{2}\left(h_{1}(h_{3} - 1)p - A\left(h_{2} + \frac{\zeta}{2}h_{3}\right) - h_{2}^{2} + \wp_{3}\tau h_{4}\right)$$

$$- Rh_{5} - \kappa h_{5} Fr = 0,$$
(21)

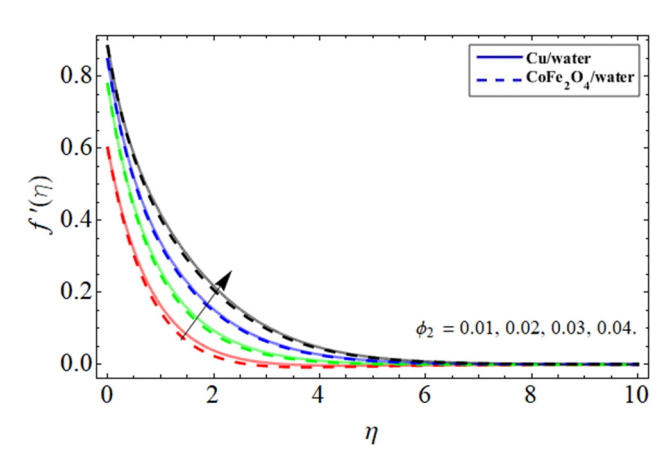


Figure 3: Velocity outlines $f'(\eta)$ vs CoFe₂O₄ NPs.

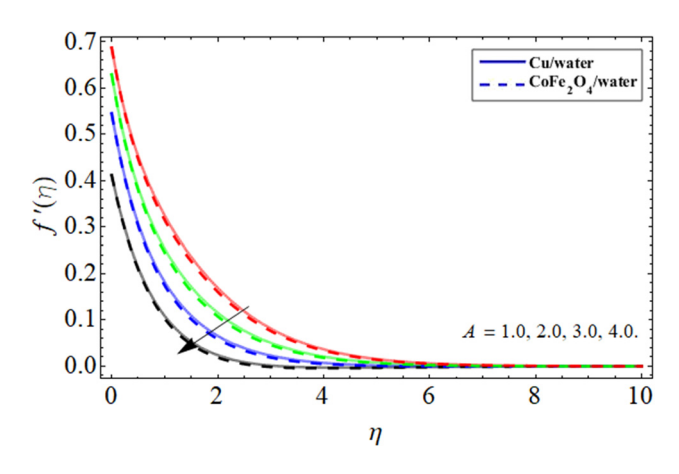
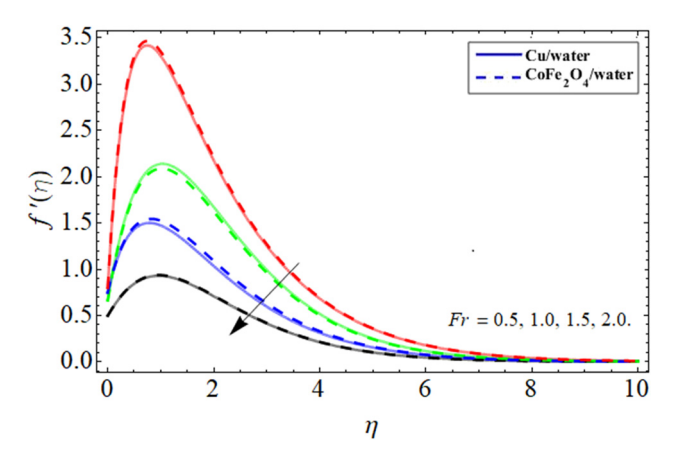


Figure 4: Velocity outlines $f'(\eta)$ vs unsteadiness constraint.

Figure 7: Velocity outlines $f'(\eta)$ vs Grashof number.



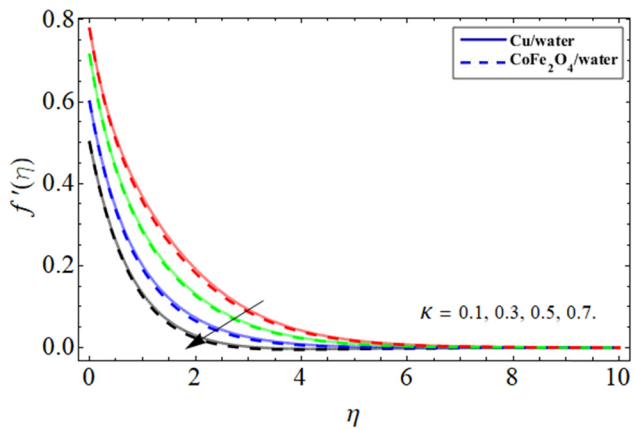
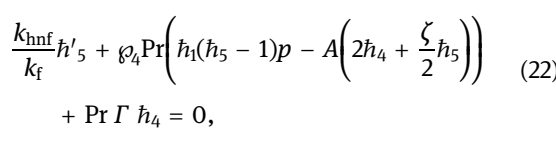


Figure 5: Velocity outlines $f'(\eta)$ vs Darcy Forchheimer number.

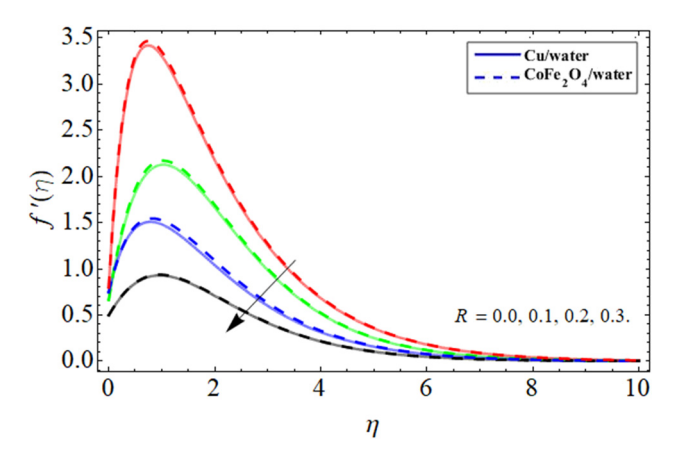
Figure 8: Velocity outlines $f'(\eta)$ vs permeability term.



$$\frac{D_{\rm hnf}}{D_f} \frac{1}{\rm Sc} \hbar'_7 + A f(\hbar_7 - 1) p - K c \hbar_6 = 0.$$
 (23)

Step 3: Applying Cauchy principal

Equations (21)–(23) are further discretized and manipulated through PCM Matlab code.



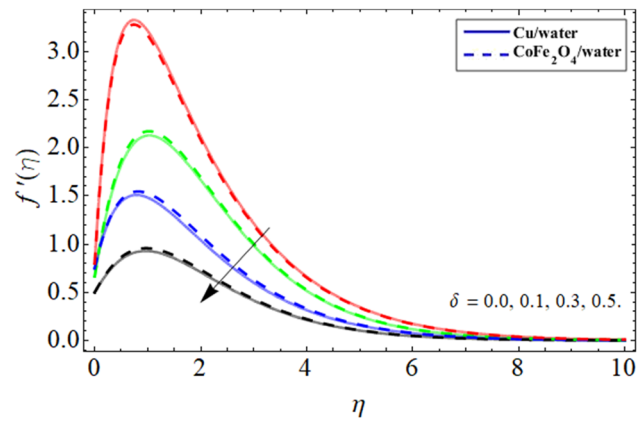


Figure 6: Velocity outlines $f'(\eta)$ vs variable viscosity term.

Figure 9: Velocity outlines $f'(\eta)$ vs second-order slip constraint.

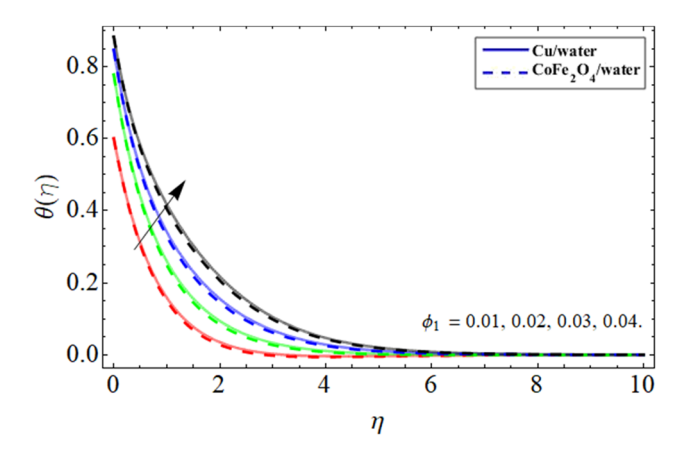


Figure 10: Energy outlines $\theta(\eta)$ vs Cu NPs.

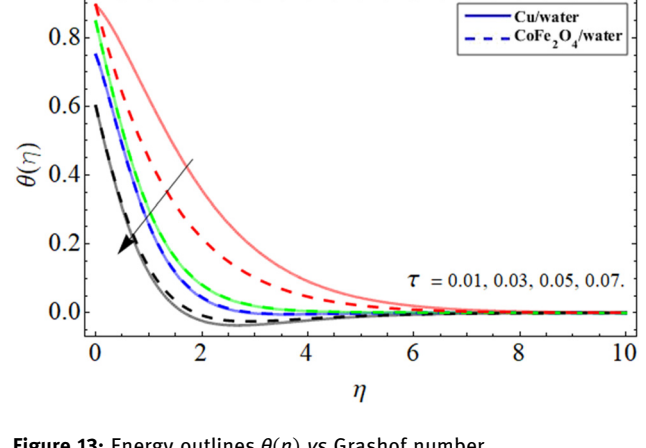


Figure 13: Energy outlines $\theta(\eta)$ vs Grashof number.

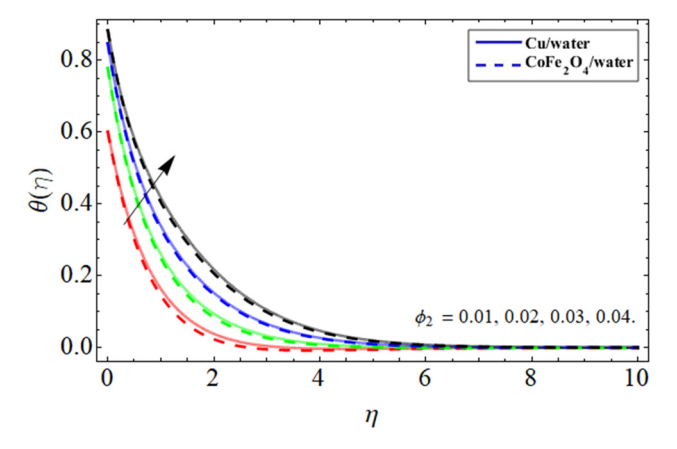


Figure 11: Energy outlines $\theta(\eta)$ vs CoFe₂O₄ NPs.

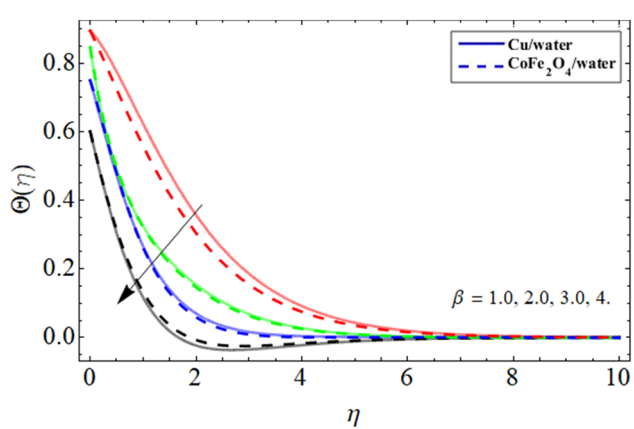


Figure 14: Energy outlines $\theta(\eta)$ vs thermal slip term.

4 Results and discussion

The purpose of this section is to explain the physics behind the graphical results and tables. Results are displayed using figures. Cu NF is represented by solid lines,

while CoFe₂O₄ NF is represented by dashes. The mechanical process of hybrid NF flow across a permeable elongating sheet is described in Figure 1. The

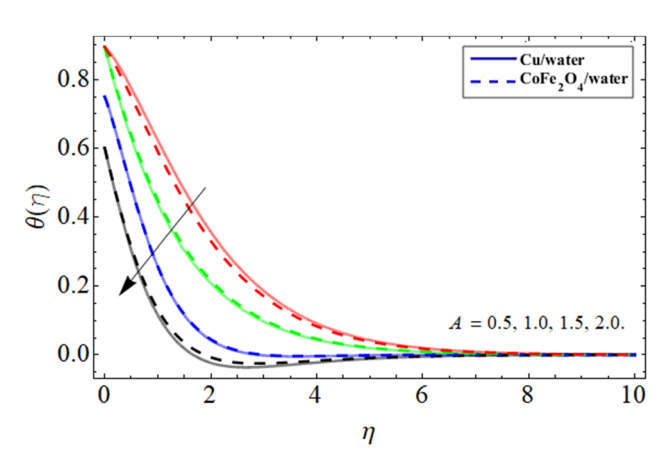


Figure 12: Energy outlines $\theta(\eta)$ vs unsteadiness term.

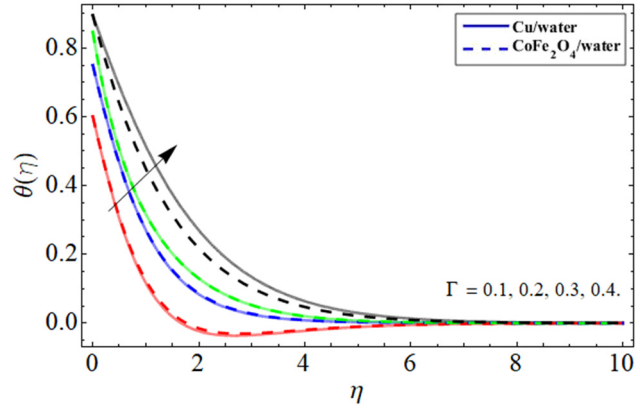


Figure 15: Energy outlines $\theta(\eta)$ vs heat absorption/generation constraint.

8 — Saqib Murtaza et al. DE GRUYTER

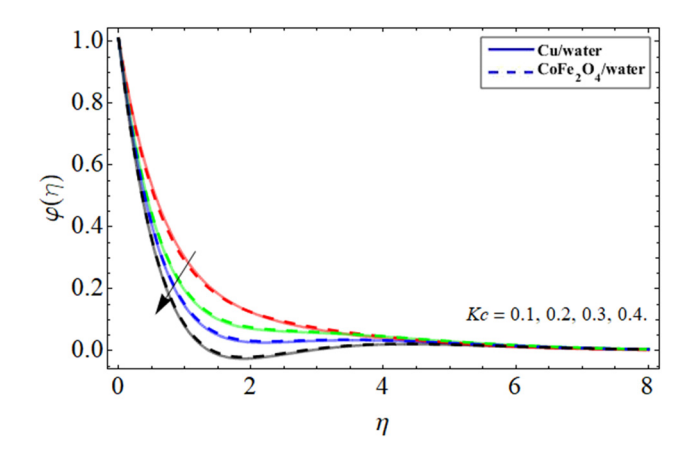


Figure 16: Energy outlines $\theta(\eta)$ vs chemical reaction.

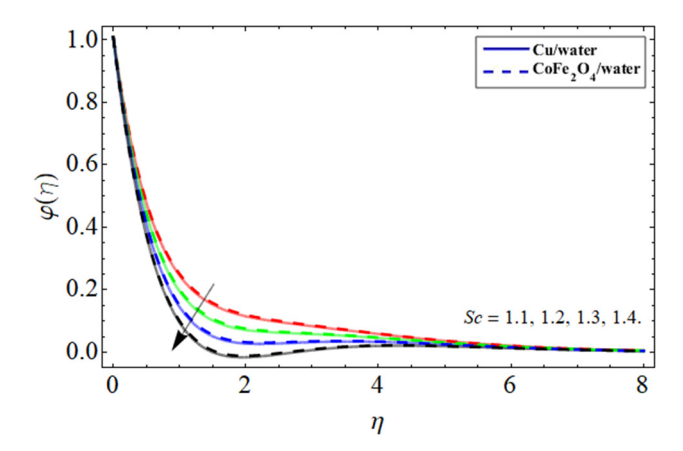


Figure 17: Energy outlines $\theta(\eta)$ vs Schmidt number.

default values of parameters are taken as A=1.0, $\phi_1=\phi_2$ =0.01, Fr = 0.5, R=0.1, $\tau=0.01$, $\kappa=\delta=0.1$, $\beta=0.2$, $\Gamma=0.1$.

Figures 2–9 highlight the behavior of velocity $f'(\eta)$ outlines vs Cu NPs, CoFe₂O₄ NPs, unsteadiness term A, Forchheimer number Fr, variable viscosity R, Grashof

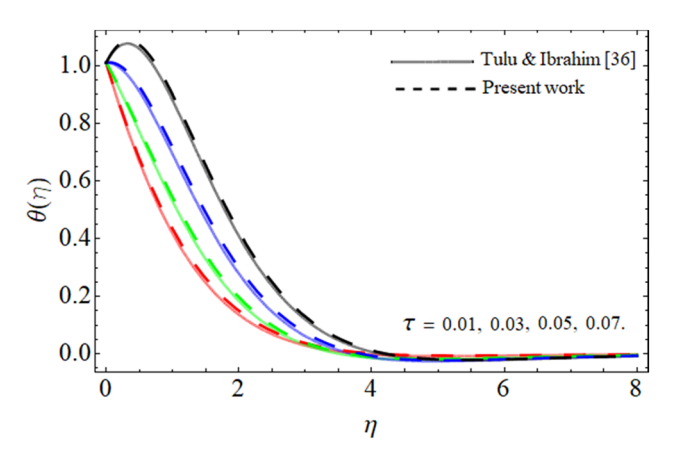


Figure 18: Validation of the present outcome with the published work.

Table 3: Statistical assessments of Sherwood and Nusselt numbers

| | PC | :M | BVP4C | | |
|------|---------------|---------------|---------------|------------------------|--|
| η | 0 ′(0) | φ ′(0) | θ' (0) | φ ′(0) | |
| 0.00 | 1.4854 | 1.5953 | 1.4781 | 1.5934 | |
| 0.03 | 1.3562 | 1.5361 | 1.3232 | 1.5315 | |
| 0.06 | 1.2482 | 1.4481 | 1.2221 | 1.4217 | |
| 0.09 | 1.0114 | 1.2010 | 2.0073 | 1.1032 | |

number τ , permeability factor κ , and second-order slip δ , respectively. Figures 2 and 3 reveal that the velocity contour enhances with the inclusion of ϕ_1 and ϕ_2 NPs. Because water has a significantly higher specific heat capability than Cu and CoFe₂O₄ NPs, while having a lower thermal efficiency, the addition of hybrid NPs, particularly Cu, diminishes its average heat-absorbing efficiency, resulting in an increase in velocity field. Figures 4 and 5 reveal that the velocity outlines decline with the upshot of unsteadiness term A and Forchheimer number Fr. Figures 6 and 7 describe that the velocity curve

Table 4: Relative comparison of the present outcomes vs the published literature

| Parameters | | Hayat <i>et al</i> . [41] | Khashi'ie et al. [42] | Present work | Hayat <i>et al</i> . [41] | Khashi'ie et al. [42] | Present work |
|------------|-----|---------------------------|-----------------------|--------------|---------------------------|-----------------------|--------------|
| М | S | f"(0) | | | f"(1) | | |
| 0.0 | 0.5 | -7.412153 | -7.4121525 | -7.4121531 | 4.714303 | 4.7143028 | 4.7143032 |
| 1.0 | | -7.592618 | -7.5926177 | -7.5926182 | 4.738017 | 4.7380165 | 4.7380173 |
| 4.0 | | -8.111334 | -8.1113342 | -8.1113361 | 4.821251 | 4.8212511 | 4.8212543 |
| 9.0 | | -8.911096 | -8.9110956 | -8.9110971 | 4.965870 | 4.9658698 | 4.9658723 |
| | 0.0 | -4.588891 | -4.5888911 | -4.5888942 | 1.843447 | 1.8434469 | 1.8434483 |
| | 0.3 | -6.666662 | -6.6666620 | -6.6666647 | 3.654695 | 3.6546948 | 3.6546974 |
| | 0.6 | -8.852444 | -8.8524442 | -8.8524462 | 5.392248 | 5.3922475 | 5.3922488 |
| | 1.0 | -11.949584 | -11.9495843 | -11.9495873 | 7.594426 | 7.5944262 | 7.5944291 |

Table 5: Numerical values for Nusselt number $\theta'(0)$

| Parameters | | | | | NF | Hybrid |
|------------|----------|-----|-----|-----|----------------------------------|-------------------------------------|
| ϕ_1 | ϕ_1 | τ | β | Pr | CoFe ₂ O ₃ | Cu-CoFe ₂ O ₃ |
| 0.01 | 0.01 | 0.2 | 0.1 | 6.2 | 2.1327595 | 2.3327595 |
| 0.02 | | | | | 2.0074208 | 2.2074204 |
| 0.03 | | | | | 1.4196705 | 1.5196702 |
| 0.04 | 0.01 | | | | 2.8247303 | 2.9247305 |
| | 0.02 | | | | 2.5824944 | 2.5824976 |
| | 0.03 | | | | 1.1319745 | 1.2319784 |
| | 0.04 | 0.2 | | | 1.9454874 | 1.9454974 |
| | | 0.3 | | | 2.5824944 | 2.6825692 |
| | | 0.4 | | | 2.1300553 | 2.3302493 |
| | | 0.5 | 0.1 | | 2.0984188 | 2.2984354 |
| | | | 0.3 | | 2.5824944 | 2.7826235 |
| | | | 0.5 | | 1.5330137 | 1.6335359 |
| | | | 0.7 | 6.2 | 1.1675688 | 1.4697365 |
| | | | | 6.4 | 0.8303698 | 1.9342547 |
| | | | | 6.6 | 1.6068036 | 2.6268491 |
| | | | | 6.8 | 2.4090316 | 3.4509078 |

declines with the upshot of variable viscosity R, while enhancing Gr. Over time the viscosity of fluid develops, which produces resistance opposite to the flow field, that's why this phenomenon happened as shown in Figure 6. Physically, the heat generation capability of the fluid improves with the effect of Grashof number, which results in the enhancement of fluid velocity. Figures 8 and 9 display that the velocity field lessens under the impact of permeability factor κ and second-order slip δ . The second-order slip component improves fluid motion resistance, reducing the fluid flow field and the thickness

Table 6: Numerical values for Sherwood number $\varphi'(0)$

| | Par | ameter | S | NF | Hybrid | |
|----------|----------|--------|-----|-----|----------------------------------|---------------------------------------|
| ϕ_1 | ϕ_1 | Кс | Sc | Pr | CoFe ₂ O ₃ | Cu – CoFe ₂ O ₃ |
| 0.01 | 0.01 | 0.2 | 0.1 | 6.2 | 3.327573 | 2.3275956 |
| 0.02 | | | | | 3.07428 | 2.074205 |
| 0.03 | | | | | 2.196723 | 1.196704 |
| | 0.01 | | | | 3.247323 | 2.347306 |
| | 0.02 | | | | 3.824943 | 2.824977 |
| | 0.03 | | | | 2.319746 | 1.319785 |
| | | 0.1 | | | 2.454875 | 1.454975 |
| | | 0.4 | | | 3.824945 | 2.825693 |
| | | 0.7 | | | 3.300554 | 2.302494 |
| | | | 0.1 | | 3.984189 | 2.984355 |
| | | | 0.2 | | 3.824945 | 2.826236 |
| | | | 0.3 | | 2.330138 | 1.335378 |
| | | | | 6.2 | 2.675689 | 1.697376 |
| | | | | 6.4 | 1.303699 | 1.342564 |
| | | | | 6.6 | 2.068038 | 2.268582 |

of the momentum boundary layer. Furthermore, a higher value δ improves the energy transference.

Figures 10-15 report the compartment of energy contour against the variation in Cu, CoFe₂O₄, unsteadiness term A, Grashof number τ , thermal slip β , heat source term Γ , respectively. Figures 10 and 11 depict that the variation in Cu and CoFe₂O₄ boosts the energy transference rate. The addition of Cu and CoFe2O4 reduces the average heat capacity of hybrid NF, which causes an advancement of the energy outline. Figures 12 and 13 emphasize that the energy curve decreases with the upshot of unsteadiness term A and Grashof number. Free convection flows are continuously carried from the stretched surface to the free stream and a rise in τ shows that free convection is progressing currents of convection. Figures 14 and 15 report that the energy curve diminishes with the outcome of thermal slip term β and enhances with the action of the heat source term. The impact of heat source term encourages fluid particles and increases their kinetic energy, which results in the elevation of the energy field.

Figures 16 and 17 reveal the mass transmission trend vs the variation in chemical reaction Kr and Schmidt number Sc. It has been noticed from Figures 16 and 17 that the mass propagation profile significantly declines with the variation in Kr and Sc. It is believed that the growing values of Sc and Kr reduce the mass outline. Figure 18 ensures the accuracy of the present results with the published work, while using the value of $\beta=0$ for no slip condition.

Tables 1 and 2 show Cu and $CoFe_2O_4$ NPs and their thermochemical properties, respectively. To confirm the validity of the current report, Table 3 presents the quantitative evaluation of PCM and BVP4C approaches. In the calculation, the heat and momentum domains are related. Table 4 expresses the relative comparison between the present results and the published literature. It can be observed that the present outcomes are accurate and reliable. Tables 5 and 6 illustrate the numerical outputs for Nusselt number and Sherwood number vs the variation in physical parameters.

5 Conclusion

An extended surface of Cu–CoFe₂O₄/H₂O hybrid NFs has been studied to determine its flow and heat transmission characteristics. Reliability substitutions are used to summarize the modeled equations of the problem. The obtained set of differential equations is further processed

computationally by employing the PCM approach. This methodology is highly accurate and fast converging. The proposed model has promising implications in biological domains such as cancer therapy, enzymatic biosensors, and drug delivery. The key conclusions of this study are as follows:

- The energy and velocity contour significantly enhances with the variation in Grashof number, Cu nanomaterials $\phi_1 = \phi_{\text{Cu}}$ and CoFe₂O₄ $\phi_2 = \phi_{\text{CoFe}_2O_4}$ nano particulates.
- The influence of permeability factor κ and second-order slip δ diminishes the velocity field.
- The velocity field declines with the effect of unsteadiness term *A*, variable viscosity *R*, and Forchheimer number *Fr*.
- The energy profile decreases with the upshot of unsteadiness term A, Grashof number, thermal slip term β , and enhances with the action of the heat source.
- The mass propagation profile significantly declines with the variation in a chemical reaction and Schmidt number.
- The inclusion of Cu and CoFe₂O₄ nanosize crystals has a huge tendency to boost the energy transmission for the biomedical and industrial purposes.
- In future, the present model may be modified to non-Newtonian fluid and can be solved with the other numerical, analytical, and fractional techniques.

Acknowledgments: The authors acknowledge the financial support provided by the Center of Excellence in Theoretical and Computational Science (TaCS-CoE), KMUTT. Saqib Murtaza is supported by the Petchra Pra Jom Klao Ph.D. Moreover, this research project is supported by Thailand Science Research and Innovation (TSRI) Basic Research Fund: Fiscal year 2023 under project number FRB660073/0164.

Funding information: The financial support is provided by the Center of Excellence in Theoretical and Computational Science (TaCS-CoE), KMUTT. Saqib Murtaza is supported by the Petchra Pra Jom Klao Ph.D. Moreover, this research project is supported by Thailand Science Research and Innovation (TSRI) Basic Research Fund: Fiscal year 2023 under project number FRB660073/0164.

Author contributions: All authors have accepted responsibility for the entire content of this manuscript and approved its submission.

Conflict of interest: The authors state no conflict of interest.

Data availability statement: The authors confirm that the data supporting the findings of this study are available within the article.

References

- [1] Mjankwi MA, Masanja VG, Mureithi EW, James MNO. Unsteady MHD flow of nanofluid with variable properties over a stretching sheet in the presence of thermal radiation and chemical reaction. Int J Math Math Sci. 2019;2019:1–14.
- [2] Gul T, Khan A, Bilal M, Alreshidi NA, Mukhtar S, Shah Z, et al. Magnetic dipole impact on the hybrid nanofluid flow over an extending surface. Sci Rep. 2020;10(1):1–13.
- [3] Bilal M, Saeed A, Selim MM, Gul T, Ali I, Kumam P. Comparative numerical analysis of Maxwell's time-dependent thermo-diffusive flow through a stretching cylinder. Case Stud Therm Eng. 2021;27:1–11.
- [4] Puneeth V, Manjunatha S, Madhukesh JK, Ramesh GK. Three dimensional mixed convection flow of hybrid Casson nanofluid past a non-linear stretching surface: A modified Buongiorno's model aspects. Chaos Solitons Fractals. 2021;152:111428.
- [5] Hussain A, Arshad M, Rehman A, Hassan A, Elagan SK, Ahmad H, et al. Three-dimensional water-based magnetohydrodynamic rotating nanofluid flow over a linear extending sheet and heat transport analysis: A numerical approach. Energies. 2021;14(16):5133.
- [6] Shuaib M, Bilal M, Khan MA, Malebary SJ. Fractional analysis of viscous fluid flow with heat and mass transfer over a flexible rotating disk. Comput Model Eng Sci. 2020;123(1):377–400.
- [7] Raza J, Dero S, Lund LA, Omar Z. Duality and stability of MHD Darcy-Forchheimer porous medium flow of rotating nanofluid on a linear shrinking/stretching sheet: Buongiorno model. Int J Numer Methods Heat Fluid Flow. 2021;9(2023):1–19.
- [8] Uddin Z, Vishwak KS, Harmand S. Numerical duality of MHD stagnation point flow and heat transfer of nanofluid past a shrinking/stretching sheet: Metaheuristic approach. Chin J Phys. 2021;73:442-61.
- [9] Rasool G, Shafiq A, Alqarni MS, Wakif A, Khan I, Bhutta MS. Numerical scrutinization of Darcy-Forchheimer relation in convective magnetohydrodynamic nanofluid flow bounded by nonlinear stretching surface in the perspective of heat and mass transfer. Micromachines. 2021;12(4):374.
- [10] Upreti H, Pandey AK, Uddin Z, Kumar M. Thermophoresis and Brownian motion effects on 3D flow of Casson nanofluid consisting microorganisms over a Riga plate using PSO: A numerical study. Chin J Phys. 2022;78:234-70.
- [11] Joshi N, Upreti H, Pandey AK. MHD Darcy-Forchheimer Cu-Ag/ H₂O-C₂H₆O₂ hybrid nanofluid flow via a porous stretching sheet with suction/blowing and viscous dissipation. Int J Comput Methods Eng Sci Mech. 2022;23(6):1–9.
- [12] Upreti H, Pandey AK, Kumar M. Unsteady squeezing flow of magnetic hybrid nanofluids within parallel plates and entropy generation. Heat Transfer. 2011;50(1): 105-25.
- [13] Waqas H, Imran M, Muhammad T, Sait SM, Ellahi R. Numerical investigation on bioconvection flow of Oldroyd-B nanofluid

- with nonlinear thermal radiation and motile microorganisms over rotating disk. J Therm Anal Calorim. 2021;145(2).
- [14] Mussabayeva B, Murzagulova K, Aripzhanova Z, Klivenko A. Preparation of silver and copper nanoparticles for biomedical application. 2017 IEEE 7th International Conference Nanomaterials: Application & Properties (NAP). IEEE; 2017, September. p. 04NB20-1.
- [15] Kart HH, Yildirim H, Kart SO, Çağin T. Physical properties of Cu nanoparticles: A molecular dynamics study. Mater Chem Phys. 2014;147(1-2):204-12.
- [16] Munjal S, Khare N, Nehate C, Koul V. Water dispersible CoFe₂O₄ nanoparticles with improved colloidal stability for biomedical applications. J Magn Magn Mater. 2016;404:166-9.
- [17] Nica V, Caro C, Páez-Muñoz JM, Leal MP, Garcia-Martin ML. Bi-magnetic core-shell CoFe₂O₄@ MnFe₂O₄ nanoparticles for in vivo theranostics. Nanomaterials. 2020;10(5):907.
- [18] Bilal M, Gul T, Alsubie A, Ali I. Axisymmetric hybrid nanofluid flow with heat and mass transfer amongst the two gyrating plates. ZAMM-J Appl Math Mech/Zeitschrift für Angew Mathematik und Mechanik. 2021;101(11):e202000146.
- [19] Ramesh GK, Madhukesh JK, Prasannakumara BC, Shehzad SA, Abbasi FM. Thermodynamics examination of Fe₃O₄-CoFe₂O₄/ Water + EG Nanofluid in a Heated Plate: Crosswise and Streamwise Aspects. Arab J Sci Eng. 2021;2022(47):1-10.
- [20] Wang J, Xu YP, Qahiti R, Jafaryar M, Alazwari MA, Abu-Hamdeh NH, et al. Simulation of hybrid nanofluid flow within a microchannel heat sink considering porous media analyzing CPU stability. J Pet Sci Eng. 2022;208:109734.
- [21] Bilal M, Saeed A, Gul T, Kumam W, Mukhtar S, Kumam P. Parametric simulation of micropolar fluid with thermal radiation across a porous stretching surface. Sci Rep. 2022;12(1):1-11.
- [22] Algehyne EA, Alhusayni YY, Tassaddig A, Saeed A, Bilal M. The study of nanofluid flow with motile microorganism and thermal slip condition across a vertical permeable surface. Waves Random Complex Media. 2022;2022(1):1-18.
- [23] Shahzad F, Jamshed W, Eid MR, El Din SM, Banerjee R. Mathematical modelling of graphene-oxide/kerosene oil nanofluid via radiative linear extendable surface. Alex Eng J. 2023:70:395-410.
- [24] Daniel YS, Aziz ZA, Ismail Z, Salah F. Effects of thermal radiation, viscous and Joule heating on electrical MHD nanofluid with double stratification. Chin J Phys. 2017;55(3):630-51.
- [25] Patel VK, Pandya JU, Patel MR. Testing the influence of TiO2-Ag/water on hybrid nanofluid MHD flow with effect of radiation and slip conditions over exponentially stretching & shrinking sheets. J Magn Magn Mater. 2023;32(5):170591.
- [26] Guedri K, Mahmood Z, Fadhl BM, Makhdoum BM, Eldin SM, Khan U. Mathematical analysis of nonlinear thermal radiation and nanoparticle aggregation on unsteady MHD flow of micropolar nanofluid over shrinking sheet. Heliyon. 2023;572:1-11.
- [27] Daniel YS, Aziz ZA, Ismail Z, Salah F. Double stratification effects on unsteady electrical MHD mixed convection flow of nanofluid with viscous dissipation and Joule heating. J Appl Res Technol. 2017;15(5):464-76.

- [28] Kuttan BA, Manjunatha S, Jayanthy S, Gireesha BJ, Archana M. Effect of variable viscosity on Marangoni convective boundary layer flow of nanofluid in the presence of mixed convection. J Nanofluids. 2019;8(4):845-51.
- [29] Shafiq A, Çolak AB, Naz Sindhu T. Designing artificial neural network of nanoparticle diameter and solid-fluid interfacial layer on single-walled carbon nanotubes/ethylene glycol nanofluid flow on thin slendering needles. Int J Numer Methods Fluids. 2021;93(12):3384-404.
- [30] Udawattha DS, Narayana M, Wijayarathne UPL. Predicting the effective viscosity of nanofluids based on the rheology of suspensions of solid particles. J King Saud Univ-Sci. 2019;31(3):412-26.
- [31] Halim N, Haq RU, Noor N. Active and passive controls of nanoparticles in maxwell stagnation point flow over a slipped stretched surface. Meccanica. 2016;52:1527-39.
- [32] Krishnamurthy M, Gireesha B, Prasannakumara B, Gorla RSR. Thermal radiation and chemical reaction effects on boundary layer slip flow and melting heat transfer of nanofluid induced by a nonlinear stretching sheet. Nonlinear Eng. 2016:5(3):147-59.
- [33] Oyelakin IS, Mondal S, Sibanda P. Unsteady Casson nanofluid flow over a stretching sheet with thermal radiation, convective and slip boundary conditions. Alex Eng J. 2016;55(2):1025-35.
- Tlili I, Khan WA, Khan I. Multiple slips effects on MHD SA-Al₂O₃ and SA-Cu non-Newtonian nanofluids flow over a stretching cylinder in porous medium with radiation and chemical reaction. Results Phys. 2018;8:213-22.
- [35] Khan SU, Waqas H, Shehzad SA, Imran M. Theoretical analysis of tangent hyperbolic nanoparticles with combined electrical MHD, activation energy and Wu's slip features: a mathematical model. Phys Scr. 2019;94(12):Article ID 125211.
- [36] Tulu A, Ibrahim W. Effects of second-order slip flow and variable viscosity on natural convection flow of (CNTs-Fe₃O₄)/ water hybrid nanofluids due to stretching surface. Math Probl Eng. 2021;2021:1-18.
- [37] Ahmad S, Ali K, Rizwan M, Ashraf M. Heat and mass transfer attributes of copper-aluminum oxide hybrid nanoparticles flow through a porous medium. Case Stud Therm Eng. 2021:25:100932.
- [38] Reddy PBA. Biomedical aspects of entropy generation on electromagnetohydrodynamic blood flow of hybrid nanofluid with nonlinear thermal radiation and non-uniform heat source/sink. Eur Phys J Plus. 2020;135(10):1-30.
- [39] Shuaib M, Shah RA, Durrani I, Bilal M. Electrokinetic viscous rotating disk flow of Poisson-Nernst-Planck equation for ion transport. J Mol Liq. 2020;313:113412.
- [40] Shuaib M, Shah RA, Bilal M. Von-Karman rotating flow in variable magnetic field with variable physical properties. Adv Mech Eng. 2021;13(2):1687814021990463.
- Hayat T, Muhammad T, Qayyum A, Alsaedi A, Mustafa M. On squeezing flow of nanofluid in the presence of magnetic field effects. J Mol Liq. 2016;213:179-85.
- [42] Khashi'ie NS, Waini I, Arifin NM, Pop I. Unsteady squeezing flow of Cu-Al₂O₃/water hybrid nanofluid in a horizontal channel with magnetic field. Sci Rep. 2021;11(1):1-11.